Probing the halo structure of ^{19,17,15}C and ^{14}B

D. Bazin, W. Benenson, B. A. Brown, J. Brown,* B. Davids, M. Fauerbach,† P. G. Hansen, P. Mantica, D. J. Morrissey, C. F. Powell, B. M. Sherrill, and M. Steiner

National Superconducting Cyclotron Laboratory, Michigan State University, East Lansing, Michigan 48824

(Received 9 December 1997)

We have measured the parallel momentum distributions of outcoming fragments in the one-neutron breakup of the odd-mass carbon isotopes ^{19,17,15}C and ^{14}B. Owing to their low neutron separation energies, the study of these nuclei is of particular interest regarding the appearance of the halo phenomenon. Discrepancies between experiment and theory observed for ^{15}C and ^{14}B indicate that their halos are not as prominent as in ^{11}Be or ^{11}Li, and that core excitations start playing a role in the breakup mechanism. In ^{17}C the halo appears hindered by a d-wave neutron ground state configuration. Finally, the data on ^{19}C suggests an s-wave neutron around the 2^+ excited state in ^{18}C. [S0556-2813(98)00805-X]

PACS number(s): 25.70.Mn, 21.10.Dr, 21.60.Cs, 27.20.+n

I. INTRODUCTION

As our knowledge on nuclei far from stability deepens, it becomes more apparent that nuclear halos are a general feature of loosely bound nuclei. As the binding energy becomes smaller in the vicinity of the drip lines, the valence nucleon(s) tunnel out of the central potential, and enhance the diffuseness of the nuclear surface. Eventually, this leads to a delocalization of the valence nucleon(s) which can be pictured as a halo surrounding the core of the nucleus. The appearance of this halo is determined by the height of the potential barrier, which itself depends on the binding energy, the angular momentum and, for protons, the Coulomb potential.

In order to investigate the formation of halos in nuclei, we present the results of experiments performed on the series of nuclei ^{19,17,15}C and ^{14}B. The choice of these nuclei is motivated by their broad range of binding energies and possibly angular momentum. ^{15}C and ^{14}B have presumably very similar $l=0$ neutron shell structures, confirmed in ^{15}C by ^{14}C(d,p) reaction angular distributions [1]. The nucleus ^{19}C has been shown to be the heaviest halo nucleus so far [2], but its detailed structure remains uncertain, partly because of the large uncertainty in its mass. The structure of ^{17}C is still unknown experimentally, but shell model calculations predict a very close proximity between the s-orbit and the d-orbit in this nucleus. The known characteristics of these four nuclei are summarized in Table I. Shell model predictions are also included for those cases where no experimental assignments are available.

Shell-model calculations using the WBP interaction [3] indicate that the well known inversion of the $0d_{5/2}$ and $1s_{1/2}$ orbits in ^{15}C is reproduced by the calculation, but also that the situation for ^{17}C and ^{19}C is not so clear, and the ground states of those two nuclei could have a more complex structure. Relativistic mean-field calculations on the carbon isotopes [4] predict a deformation of the neutron-rich isotopes which peaks at ^{18}C, and ground states of $1/2^+$, $3/2^+$, and $1/2^+$ for ^{15}C, ^{17}C, and ^{19}C, respectively.

II. EXPERIMENT

A. Method

In this experiment the halo structure of the studied nuclei was probed using knockout reactions in which the valence neutron is removed from the projectile and the momentum of the recoiling core is measured. Qualitatively we then expect from the uncertainty principle that the width of the valence neutron distribution in momentum coordinates is inversely proportional to its width in space coordinates. In the sudden approximation [5], the momentum distribution in the breakup of the deuteron directly reflects its internal momentum distribution and provides a direct measurement of the Fourier transform of the internal wave function. The same technique is used in atomic physics [6] to probe the wave function of valence electrons. The presence of a strongly absorbing nuclear core in heavier nuclei modifies this picture, most strongly for the transverse component of the neutron momentum, which essentially reflects diffraction dissociation [7]. The longitudinal momentum distribution of the charged fragment (and, presumably the neutron) is expected to be less affected [8] and has been successfully used in many experiments (see for instance [9–11]), including our previous study of the halo of ^{19}C [2]. Small corrections to this picture are discussed below.

The selection of the one-neutron removal channels restricts the total reaction cross section to impact parameters

TABLE I. Characteristics of the studied nuclei. Shell model predictions have been included when the orbitals are unknown experimentally (calc.).

Nucleus	S_n	J^π g.s.	Valence neutron orbit
^{14}B	970 ±21 keV	2^- (expt.)	$1s_{1/2}$ (expt.)
^{15}C	1218.1 ±0.8 keV	$1/2^+$ (expt.)	$1s_{1/2}$ (expt.)
^{17}C	729 ±18 keV	$3/2^+$ (calc.)	$0d_{5/2}$ (calc.)
^{19}C	160 ±110 keV	$1/2^+$ (calc.)	$1s_{1/2}$ (calc.)

*Present address: Department of Physics, Allegheny College, Meadville, PA 16335.

†Present address: Department of Physics, Florida State University, Tallahassee, FL 32306.

greater than the sum of the core and target radii. Reactions leading to the breakup of the core do not contribute to the observed momentum distributions, which therefore only contain information about the outer region of the wave function. This localization or shadowing effect [12–14] leads to a modification of the momentum distribution (mostly a suppression of the high-momentum components) and a reduction of their width. It should be emphasized that this method seems valid only if there is a definite delocalization of the halo particle(s), and one can assume that the breakup reaction does not affect the core. As soon as the valence particle(s) are closer, other channels involving the core will become open and start contributing to the cross section. More complete calculations taking into account these core excitations would therefore be necessary for a complete description of experimental data.

B. Experimental details

The experiment was performed at the A1200 [15] fragment separator at the National Superconducting Cyclotron Laboratory. The secondary beams of ^{14}B, ^{15}C, and ^{17}C were produced by fragmenting an ^{18}O beam at 100 MeV/nucleon on a 790 mg/cm^2 thick Be target. Because the production cross section from ^{18}O is smaller, the ^{19}C were produced by fragmenting an ^{40}Ar beam at 100 MeV/nucleon on a 470 mg/cm^2 thick Be target. The separator was operated in dispersion-matched mode [16] in which the reaction target is placed at a dispersive location, and the intrinsic dispersion of the secondary beam is compensated for by the last section of the spectrometer. The magnetic rigidity of this last section is set according to the momentum of the outgoing core fragment.

The horizontal position of the particles at the focal plane was recorded using a Cathode Readout Drift Chamber (CRDC) filled with gas in which the primary electrons produced by the particle drift to a single wire to produce an avalanche. The charge distribution produced by this avalanche is then imaged and recorded on a series of pads located along the wire. The measured position is the centroid of the charge distribution. Behind the CRDC were two 300 μm silicon detectors which provided the energy-loss measurements and a thick plastic scintillator in which the particles stopped. The time of flight from the production target to the focal plane was measured between the plastic scintillator and the rf-cyclotron signal.

As fragment separation was provided by the first section of the spectrometer, the selection of the fragments was in magnetic rigidity only, which introduced numerous contaminants in the secondary beams. However, this allowed some of the nuclei of interest to be transmitted simultaneously, such as ^{14}B and ^{17}C which were transmitted at the same Bρ setting. Although other reactions and scattered particles from the contaminants arrived at the focal plane, the group of events corresponding to the one-neutron breakup of the nuclei of interest was uniquely identified because of its unique time of flight and the specific setting of the magnetic rigidities of the A1200. The elastically scattered $^{A-1}$Z nuclei were not transmitted through the last section of the spectrometer because their momentum did not match the rigidity.

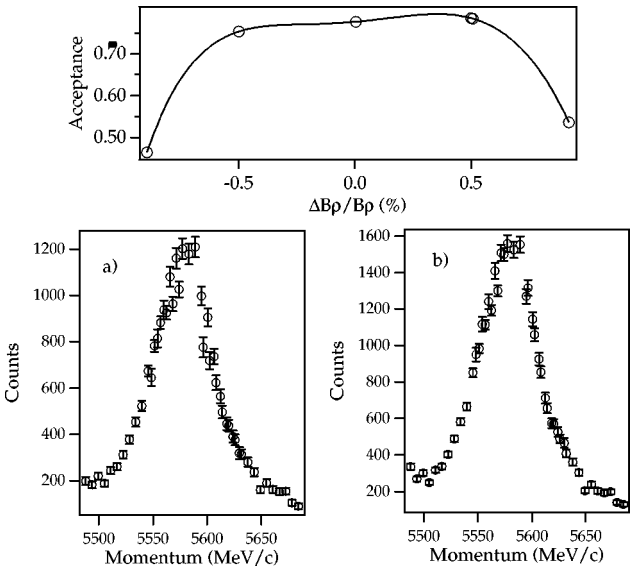

FIG. 1. Top: momentum acceptance of the A1200 spectrometer. The curve has been used to correct the data for each momentum bin of the distributions. Bottom: example of an uncorrected (a) and corrected (b) momentum distribution. The distribution consists of three momentum bins pieced together.

The reaction targets of Be and Ta had thicknesses of 190 mg/cm^2 and 295 mg/cm^2 respectively, chosen for equivalent energy loss. The situation is particularly favorable in the case of a neutron stripping reaction, since the differential energy loss between ^{A}Z and $^{A-1}$Z is very small. The thickness limitation was the energy straggling, chosen to be about the same magnitude as the resolution of the spectrometer. The momentum dispersion and the resolution were measured by stepping the elastically scattered secondary beam across the focal plane. This also allowed the mapping of the acceptance of the last section of the A1200. The momentum resolution was 0.12% with the Be target and 0.16% with the Ta target, which would correspond for the ^{15}C breakup to 6.7 MeV/c and 9.0 MeV/c FWHM, respectively.

The beam intensity was monitored by a set of small silicon detectors located near the production target. The ratio between the number of incoming nuclei of interest and the beam monitors was measured by transmitting the secondary beam directly to the focal plane. This ratio was later used to determine the breakup cross sections.

C. Data analysis

On the top of Fig. 1 is shown the shape of the measured momentum acceptance. As can be seen from the figure, it is flat in a momentum range of about 1% and therefore limits the extent to which the tails of the momentum distribution can be measured. For this reason, the measurement of ^{15}C, ^{14}B and ^{17}C consisted of 3 magnetic rigidity settings at intervals -1%, 0%, and 1% from the calculated momentum of the core fragments. The reconstruction of the final momentum distribution was performed using the acceptance mapping as well as the normalization of secondary beam intensity for each setting. An example of such a reconstruction is shown in Fig. 1, taken from the breakup of ^{15}C on the Be target. In the left spectrum one clearly sees the effect of the limited acceptance for the overlap regions between the set-

tings of the spectrometer. After correction (spectrum on the right), the overlap regions show a much better agreement between each setting.

The limited angular acceptance of the last section of the A1200 spectrometer can modify the shape of the parallel momentum distributions after integration over the transverse dimensions. However, this modification depends on whether the initial shape of the 3-dimensional distribution factorizes or not. If the initial shape is close to a Gaussian, then the transverse and parallel components are independent and there is no modification. If the distribution is closer to a Lorentzian, then a partial integration of p_x and p_y in the intervals $|p_{x\mathrm{lim}}|=\langle p_z\rangle\times \sin(\Delta\theta/2)$ and $|p_{y\mathrm{lim}}|=\langle p_z\rangle \times \sin(\Delta\phi/2)$ where $\Delta\theta$ and $\Delta\phi$ are the horizontal and vertical acceptances, respectively, leads to the following line shape for the p_z distribution:

$$\frac{d\sigma}{dp_z}\equiv\frac{1}{(p_z-\langle p_z\rangle)^2+(\hbar/\rho)^2}\left[\frac{p_{x\mathrm{lim}}\arctan[p_{y\mathrm{lim}}/\sqrt{p_{x\mathrm{lim}}^2+(p_z-\langle p_z\rangle)^2+(\hbar/\rho)^2}]}{\sqrt{p_{x\mathrm{lim}}^2+(p_z-\langle p_z\rangle)^2+(\hbar/\rho)^2}}+\frac{p_{y\mathrm{lim}}\arctan[p_{x\mathrm{lim}}/\sqrt{p_{y\mathrm{lim}}^2+(p_z-\langle p_z\rangle)^2+(\hbar/\rho)^2}]}{\sqrt{p_{y\mathrm{lim}}^2+(p_z-\langle p_z\rangle)^2+(\hbar/\rho)^2}}\right], \tag{1}$$

where ρ is the decay length inversely proportional to the Lorenztian width of the distribution: $\rho=2\hbar/\Gamma$. At the limit where $p_{x\mathrm{lim}}$ and $p_{y\mathrm{lim}}$ go to infinity, the term in brackets does not depend on p_z anymore leading to a Lorentzian line shape. These effects are studied in more detail in [17]. In medium acceptance mode, the $\Delta\theta$ and $\Delta\phi$ angular acceptances of the A1200 [15] are 20 mrad and 40 mrad, respectively. These values are used with the modified Lorentzian line shape to fit the data and extract directly the Lorentzian width corrected from the angular acceptance cut. It should be emphasized that this method of extracting a width from the data is model dependent since it assumes a Lorentzian for the shape of the distribution, which corresponds only to the case of an $l=0$ single particle wave function and assumes the absence of the shadowing effect discussed above. In the following calculations, the effect of the geometrical acceptance of the spectrometer is taken into account whenever relevant.

III. CALCULATIONS

A. Hankel wave functions

The first calculation used in the comparison to the nuclear breakup data uses Hankel wave functions which are the exact solution of the Schrödinger equation outside the range of the potential. It is assumed that the radius of light targets is small compared to the scale of the wave function, which is replaced by its value at the center of the target. The details of the calculation are given in [12]. The expressions derived analytically have been found to be within 1% of the results obtained by a numerical calculation using a Woods-Saxon potential [12]. We have extended the calculation to the case of a d-state, needed for comparison with the ^{17}C data. Following the notation in [12], we obtain for the probability distribution as a function of the momentum along the z axis and for $l=2$:

$$\frac{dW_2}{dk_z}=\frac{\sigma_T B^2}{8\pi^2\kappa^3}[(3k_z^2+\kappa^2)^2K_0^2(\chi)+12k_z^2(k_z^2+\kappa^2)K_1^2(\chi)+3(k_z^2+\kappa^2)^2K_2^2(\chi)] \tag{2}$$

in which σ_T is the free nucleon cross section, B a dimensionless constant obtained, in principle by matching the Hankel wave function to the internal solution obtained, e.g., from a Woods-Saxon wave function, κ the range in momentum space obtained from the reduced mass and separation energy through $\kappa=\sqrt{2\mu S_n}/\hbar$ and χ the argument of the modified Bessel functions $\chi=b\sqrt{\kappa^2+k_z^2}$. The impact parameter is denoted by b. The 3 terms in the probability distribution correspond to the contributions from $m=0$, $m=\pm1$ and $m=\pm2$ respectively, the last being the most important. After integration over the impact parameter, the differential cross section is

$$\frac{d\sigma_2}{dk_z}=\frac{\sigma_T B^2 b_{\min}^2}{8\pi\kappa^3}\left[(3k_z^2+\kappa^2)^2(K_1^2-K_0^2)+12k_z^2(k_z^2+\kappa^2)\left(K_2^2-K_1^2-\frac{2}{\xi}K_1K_2\right)+3(k_z^2+\kappa^2)^2\left(K_3^2-K_2^2-\frac{4}{\xi}K_2K_3\right)\right], \tag{3}$$

where the argument of the modified Bessel functions K_i is $\xi=b_{\min}\sqrt{\kappa^2+k_z^2}$. The minimum impact parameter $b_{\min}$ is the sum of the core and target radii, chosen to reproduce heavy-ion interaction cross sections. The halo breakup cross section can be deduced by integrating the differential cross section along the parallel momentum axis.

B. Shell model mixing and Woods-Saxon wave functions

In the second calculation presented in this paper, we have used shell model calculations to determine the parentage of the ground state to single particle wave functions. These wave functions are calculated using a Woods-Saxon potential with radius and diffuseness parameters $r_0=1.25$ fm and $a=0.7$ fm, the well depth being adjusted to reproduce the binding energy. The localization effect is calculated numerically and yields parallel momentum distributions which are subsequently summed according to their relative contribution to the ground state. For pure single particle ground states, the

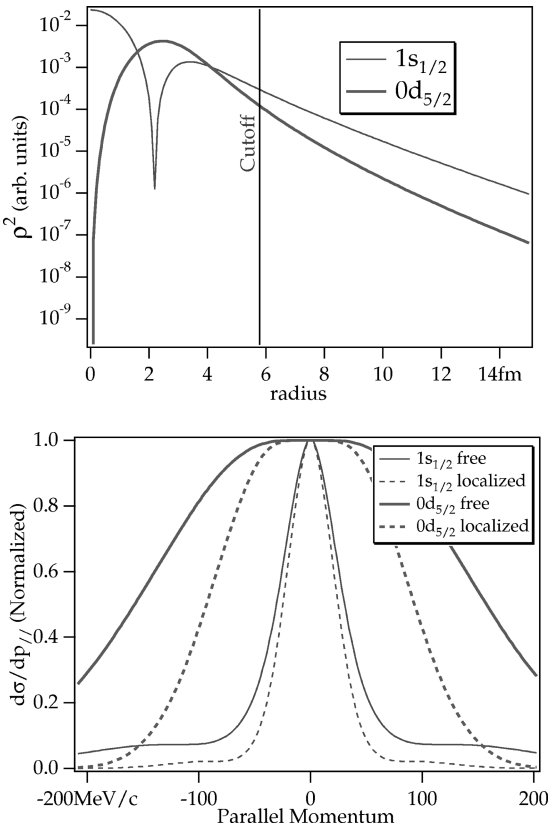

FIG. 2. $0d_{5/2}$ and $1s_{1/2}$ wave functions calculated in a Woods-Saxon potential and their corresponding parallel momentum distributions with (dashed line) and without (plain line) a localization effect. The calculation assumes a neutron separation energy of 970 keV.

results are similar to those obtained with the Hankel calculation presented in the previous section.

Figure 2 shows an example of wave functions and their corresponding parallel momentum distributions with (dashed line) and without (full drawn line) localization for $0d_{5/2}$ and $1s_{1/2}$ orbits. The only part of the wave functions left at radii greater than the cutoff are the exponential tails, which are essentially identical to the Hankel wave functions of the previous section. Because of the centrifugal barrier, the tail of the *s* orbit wave function extends farther out than that of the *d* orbit, and the localization effect leads to a greater reduction of the *d* orbit momentum distribution than the *s* orbit (the maxima of the distributions have been normalized to unity in the figure to better show the width modification due to the localization). This means that even a small component of *s* orbit in a wave function can play an important role in the final momentum distribution, whereas a *d* component would have to dominate in order to affect it.

IV. RESULTS AND DISCUSSION

A. Breakup of ^{15}C and ^{14}B

1. Nuclear breakup

As can be seen on Table I, ^{15}C and ^{14}B are the best known nuclei of our study set. The angular distribution from the ground state of ^{15}C in the reaction ^{14}C$(d,p)^{15}$C [1] reveals the assignment $1/2^+$. The set of optical parameters giving the best fit in a DWBA calculation also gives a spectroscopic factor of 0.88. This spectroscopic factor is in line with shell model calculations. The ground state of ^{14}B is 2^-, resulting from a hole in the $0p_{3/2}$ proton shell coupled to a single neutron in the $1s_{1/2}$ neutron shell. The neutron shell structure of ^{14}B is therefore very similar to that of ^{15}C, and a shell model calculation yields a spectroscopic factor of 0.95.

The parallel momentum distributions of ^{14}C and ^{13}B after the breakup of ^{15}C and ^{14}B on the Be target are presented in the top parts of Fig. 3. The momentum distribution from ^{14}B breakup was measured simultaneously with the ^{17}C breakup, as ^{14}B was transmitted as a contaminant in the ^{17}C secondary beam. A fit to the data with a modified Lorentzian lineshape is used to extract the experimental width (see also Table II). The dashed lines shown in the spectra obtained for nuclear breakup come from an $l=0$ Hankel function calculation with localization. A calculation using a Woods-Saxon potential gives very similar distributions. The effect of a possible *d*-component in the wave function is negligible at the level of 10%, as it is the most supressed by the localization effect. Because the binding energies of ^{15}C and ^{14}B are well known, there is very little error on the calculated width. The width of the vertical bar crossing the dashed curve represents the error due to the mass uncertainty, and is less than the line thickness.

It is apparent from Fig. 3 that the observed parallel momentum distributions from the one-neutron nuclear breakup of ^{15}C and ^{14}B are different from the predicted shapes. This comes as a surprise, since this calculation has been shown to reproduce the momentum distributions observed in the nuclear breakup of ^{11}Be and ^{8}B [12,11]. In particular, the wave function of ^{11}Be is also known to be an almost pure *s*-state, although with a different binding energy. The main discrepancy with the calculation is found in the tails of the momentum distributions, which correspond to smaller radii in spacial coordinates. A closer look at Fig. 3 reveals that this discrepancy seems more pronounced for ^{15}C than for ^{14}B. These two facts suggest that the origin of the difference between the observations and the calculations lies in contributions from the core. As the binding energy increases, the size of the halo decreases and breakup reactions where the core gets excited become possible. For the cases that we discuss here, the halo still extends far beyond the core radius of approximately 2.5 fm. A calculation with Woods-Saxon wave functions for the halo neutron gives root-mean-square radii of 5.62 fm and 5.98 fm for ^{15}C and ^{14}B, respectively. Very recent data were taken on the breakup of ^{15}C with γ-rays detected in coincidence with the fragment. They suggest that an important contribution in the neutron stripping leads to the 1^- state at 6.09 MeV in ^{14}C, which has the parentage $^{13}\mathrm{C} \otimes 1s_{1/2}$. This will explain the high-momentum tails of the distributions.

2. Coulomb breakup

The bottom spectra of Fig. 3 show the parallel momentum distributions obtained in the one-neutron breakup of ^{15}C and ^{14}B. The dashed curves show a Coulomb breakup calculation based on the analytical expressions given in [18]. As in the nuclear breakup data shown in the previous paragraph, the biggest discrepancy between the calculated and observed

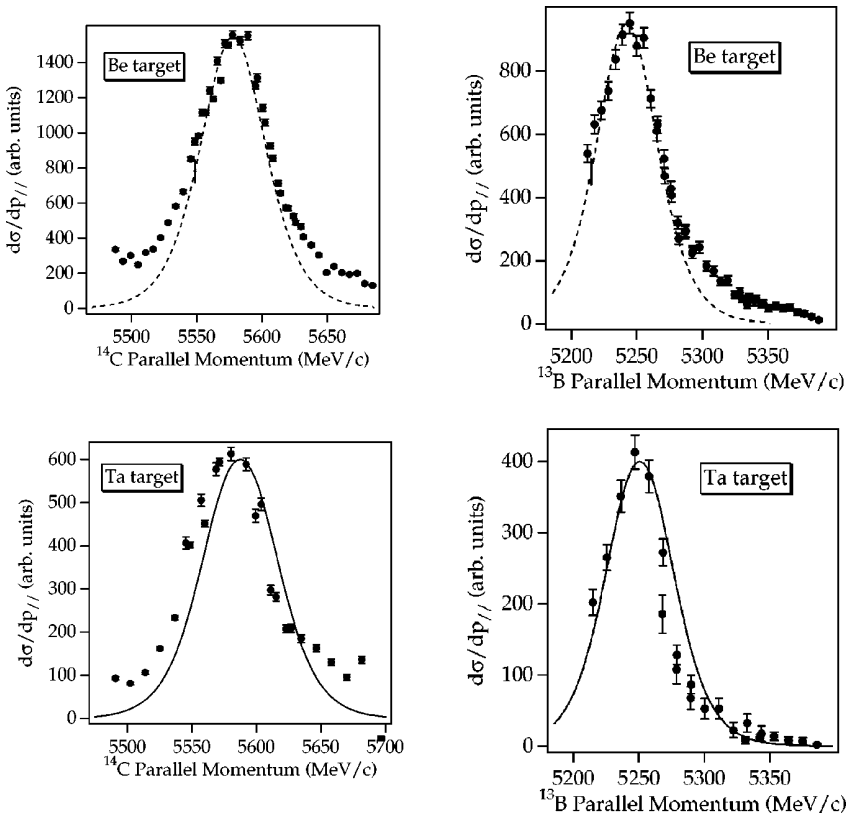

FIG. 3. Left: Unnormalized parallel momentum distribution of ^{14}C after the breakup of ^{15}C on Be (top) and Ta (bottom) targets. The dashed line in the top figures corresponds to an $l=0$ Hankel function calculation taking into account the localization effect. The solid curve in the bottom figures comes from a Coulomb breakup calculation using a Yukawa potential (see text). Right: parallel momentum distribution of ^{13}B after the breakup of ^{14}B on Be (top) and Ta (bottom) targets. The deviations between the experimental and calculated peak positions here and in Fig. 5 are within the uncertainties of the calibration.

momentum distributions lies in the tails. This again suggests that core contributions may be responsible for the discrepancy, where reactions removing a neutron from the core rather than from the halo account for a significant part of the cross section. The mismatch in absolute momentum between the experiment and the calculations is consistent with the uncertainty in the absolute calibration.

The experimental Coulomb breakup cross sections after integration over longitudinal momentum are given in Table III, where they are compared with a calculation using Woods-Saxon single-particle wave functions both for the bound s-state and for the continuum p-states. For completeness we show also the absolute cross sections obtained with a Yukawa wave function (given as set 1), the approximation that we used for calculating the shape of the momentum distributions in Fig. 3. The difference in cross section of approximately 30% illustrates that introducing a finite-size correction, here of the order of a factor 2, gives less precise estimates than was the case for the more loosely bound ^{11}Be [7,18].

TABLE II. Measured FWHM of the parallel momentum distributions expressed in the c.m. system. The width is the Γ parameter given by Eq. (1).

Nucleus	Be target	Ta target
^{14}B	57 ± 2 MeV/c	48 ± 3 MeV/c
^{15}C	67 ± 3 MeV/c	67 ± 1 MeV/c
^{17}C	145 ± 5 MeV/c	
^{19}C	42 ± 4 MeV/c	41 ± 3 MeV/c

The most striking feature, however, is that the measured Coulomb cross sections given in Table III are factors 4–8 smaller than the calculated values, whereas the agreement was essentially exact for the case of ^{11}Be, bound by 0.5 MeV. Since we neglect nuclear contributions to the reactions with the tantalum target, the real reduction factor is likely to be larger. We believe that this primarily reflects the increasing influence of the giant dipole resonance with increasing separation energy of the halo neutron, 0.97 and 1.22 MeV for ^{14}B and ^{15}C, respectively, so that we are seeing the onset of the quenching of the low-energy $E1$ strength. This is qualitatively what is expected for the behavior of the soft dipole mode of a halo nucleus (which seems to be predominantly a single-particle and noncollective mode). A more quantitative comparison must, however, await the clarification of an experimental problem affecting the absolute normalization of the cross sections for Coulomb dissociation.

This problem arises from the Coulomb deflection of the projectile. If the average of the horizontal and vertical acceptance is taken to be 30 mrad, then the minimum impact parameter becomes of the order of 20 fm, which cuts the calculated Coulomb cross sections by approximately a factor 2 relative to the values given as set 2 of Table III. We hope soon to be able to carry out measurements with a spectrometer with higher angular acceptance.

TABLE III. Measured and calculated cross sections. The nuclear breakup cross sections were calculated by integrating the parallel momentum distributions obtained from the Hankel function calculations. The calculated Coulomb breakup cross sections are based on pertubation theory and represent electric dipole transitions from the bound s-state to continuum p-states. The first set uses a Yukawa potential with finite-size corrections [18,24], and the second a Woods-Saxon potential. Note that the experimental cross sections are not corrected for possible contributions from the angular acceptance of the spectrometer. The quoted errors on ^{19}C are statistical only. For the other nuclei the dominating error is systematic and is estimated around 10%. Its two most significant contributions come from the beam monitoring which did not scale linearly with intensity and the inhomogeneity of the reaction target.

Nucleus	Beam energy	Be target	Calculated nuclear	Ta target	Calculated Coulomb (1)	Calculated Coulomb (2)
^{14}B	86 MeV/u	48 mb	112 mb	157 mb	447 mb	676 mb
^{15}C	85 MeV/u	33 mb	120 mb	75 mb	394 mb	625 mb
^{17}C	84 MeV/u	26 mb	37 mb			
^{19}C	88 MeV/u	105 $\pm$17 mb	84 mb	1.1 $\pm$ 0.4 b	3.68 b	4.52 b

B. Breakup of ^{17}C

Little is known about the structure of ^{17}C. Its ground state and an excited state at 295$\pm$10 keV have been observed in the reaction ^{48}Ca(^{18}O,^{17}C) at 6.2 MeV/nucleon [19]. However, no spin assignment could be deduced from these data. Shell model calculations indicate that three closely spaced low-lying states are expected, their order varying with the interaction used in the calculations.

The parallel momentum distribution of ^{16}C core fragments from the nuclear breakup of ^{17}C on a Beryllium target is presented in Fig. 4. No useful data could be extracted from the Coulomb breakup because of background coming from the contaminants in the secondary beam. The striking feature of the spectrum displayed in Fig. 4 is the large width of the momentum distribution, which is fitted in the center-of-mass system by a modified Lorentzian line shape of width 145$\pm$5 MeV/c, despite the relatively small binding energy (see Table I). The large discrepancy between this value and the one found in our previous paper [2] is attributed to a poor identification of the ^{16}C fragments in that earlier work. Calculations using the Hankel function solutions lead to widths of 45 MeV/c and 142 MeV/c for a s-state and a d-state, respectively. These calculations point towards a predominance of a d component in the ground state of this nucleus. However, the shape of the parallel momentum distribution calculated for a pure d-state does not match the observed one (see Fig. 4).

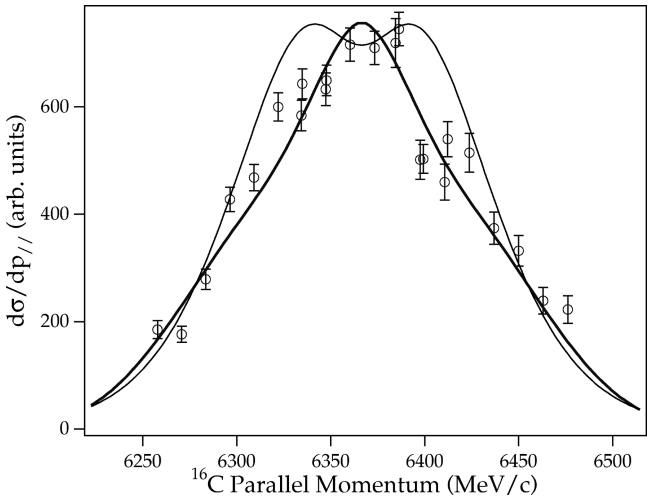

FIG. 4. Parallel momentum distribution of ^{16}C after the breakup of ^{17}C on a Be target. The thin line corresponds to an $l=2$ Hankel function calculation. The thick line is the sum of s and d components calculated with a Woods-Saxon potential and parentage coefficients of 0.16 and 1.58, respectively.

Shell model calculations suggest that both the s and d single-particle components are present in the ground state. A calculation performed with the WBP interaction [3] predicts parentage coefficients of 1.58 and 0.16 to the $0d_{5/2}$ and $1s_{1/2}$ orbits respectively, assuming a coupling to the 2^+ state of ^{16}C. The shell model ground state is $3/2^+$ and the $d_{3/2}$ parentage to the ^{16}C ground state is small. In this case the binding energy is augmented by the excitation energy of the 2^+ state, which yields 2.5 MeV instead of 0.73 MeV. Because a d-state wave function is more concentrated in the potential than an s-state wave function, the localization caused by the reaction suppresses the d component more than the s component. This effect counterbalances the parentage coefficients in the case of this calculation, and the two components give comparable contributions. The resulting momentum distribution is shown in thick line on Fig. 4, and agrees remarkably well with the data. The corresponding FWHM is listed with the experimental value in Table II.

C. Breakup of ^{19}C

As in ^{17}C, the low-lying states of ^{19}C are expected to be $0d_{5/2}$ and $1s_{1/2}$. Shell model calculations predict an s-state but some uncertainty remains due to the proximity of the $3/2^+$ and $5/2^+$ states. The β-decay of ^{19}C has been studied experimentally [20] and delayed neutron emission to excited states of ^{18}N have been observed. However, comparison of the GT strength distribution with shell model calculations does not allow a determination of the spin and parity of the ^{19}C ground state.

1. Nuclear breakup

The nuclear breakup of ^{19}C on a Be target was measured in our first experiment [2]. The data from that experiment have been revised, and the overestimated error bars have been reduced. The parallel momentum distribution of ^{18}C

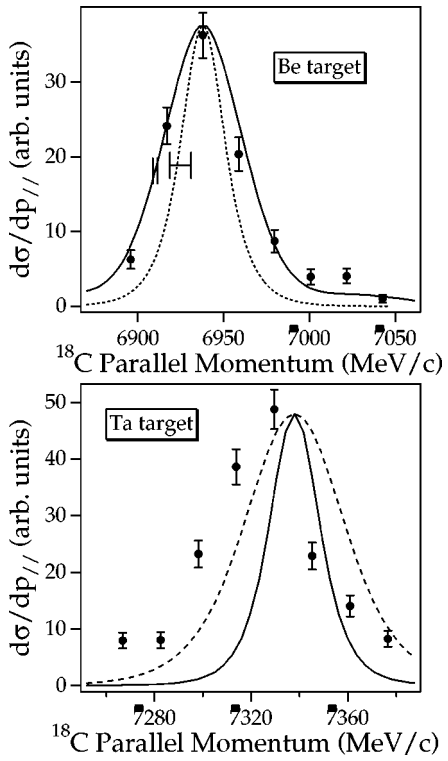

FIG. 5. Parallel momentum distribution of ^{18}C after the breakup of ^{19}C on a Be target (top) and a Ta target (bottom). The dashed line in the top figure corresponds to an $l=0$ Hankel function calculation. The large uncertainty on the width due to the error on the mass is indicated by a horizontal error bar at half maximum. The thick line is the sum of *s* and *d* components (although the *d* component is negligible in this case) calculated with a Woods-Saxon potential and parentage coefficients of 0.49 and 0.08 respectively. The curves in the bottom part of the figure correspond to a Coulomb breakup calculation using a Yukawa potential. The solid curve stands for the tabulated value $S_n=0.16$ MeV and the dashed curve for $S_n=0.6$ MeV, value needed to reproduce the data (see text).

fragments is shown on the top of Fig. 5. A fit to the modified-Lorentzian line shape yields a FWHM of 42 ± 4 MeV/*c* in the c.m. system (see Table II). Although this width clearly indicates a delocalization of the valence neutron in the form of a halo, a comparison to an $l=0$ calculation using the Hankel wave function fails to reproduce the data. The dashed line displayed on the top of Fig. 5 shows a much smaller width, even though the large uncertainty on the mass introduces a large error bar on the calculation (also displayed in the figure).

A shell model calculation using the WBT interaction predicts a $5/2^+$ spin-parity for the ground state of ^{19}C, corresponding to the coupling of an $l=0$ valence neutron to the 2^+ state in ^{18}C. In this calculation, the separation energy of the last neutron is augmented by the excitation energy of the 2^+ state, yielding 1.8 MeV. The parentage coefficients to the $1s_{1/2}$ and $0d_{5/2}$ orbits are 0.49 and 0.08, respectively. Because the *d* component is so weak and more suppressed by the localization effect than the *s* component, it can be neglected. The momentum distribution calculated using a Woods-Saxon potential is displayed on top the data in Fig. 5 and is in better agreement than the $l=0$ Hankel calculation. Due to the larger separation energy of the valence neutron, the width of the parallel momentum distribution is much less sensitive to the mass determination of ^{19}C, as indicated by the horizontal error bar. The comparison of cross sections calculated with either an *s*-orbit coupled to the 0^+ ground state or the 2^+ state of ^{18}C leads to the same conclusion. The first calculation yields 290 mb and the second 84 mb, compared to the experimental value of 105 ± 17 mb (see also Table III). The same result is also suggested by recent coupled channel calculations performed using a deformed Woods-Saxon potential [21].

2. Coulomb breakup

The parallel momentum distribution of ^{18}C from the Coulomb breakup of ^{19}C on a Ta target is displayed on the bottom of Fig. 5. The observed width is very similar to the nuclear breakup width, wih a modified-Lorentzian fit yielding a FWHM of 41 ± 3 MeV/*c*. This width is in agreement with the results from a recent experiment [22] where neutrons from the breakup of ^{19}C have been observed. The two curves are from a Coulomb breakup calculation similar to that of [18] using a Yukawa potential. The solid curve corresponds to the tabulated [23] value of $S_n=0.16 \pm 0.11$ MeV, and the dashed curve to $S_n=0.6$ MeV, value needed to reach agreement with the data. The discrepancy between calculation and experiment suggests, as for the nuclear breakup data, that the ground state wave function of ^{19}C is more complex than a simple *s*-orbit coupled to the ground state of the ^{18}C core. Although the error bar on the mass of ^{19}C is quite large, it would have to be stretched by more than 3σ to give reasonable agreement with the data.

The measured cross section is listed with the other results from this experiment in Table III. The two Coulomb breakup calculations (see Sec. IV A 2) were calculated using the value $S_n=0.16$ MeV, and also overestimate the experiment, although by a smaller factor than for ^{14}B and ^{15}C. As already mentioned in Sec. IV A 2, the discrepancy is linked to the fact that a significant part of the $E1$ strength still is going to the giant dipole resonance, but because of the large uncertainty in the neutron separation energy, a more precise comparison is not possible.

V. CONCLUSION

In this experiment, we have measured the longitudinal momenta of core fragments emitted in the one-neutron breakup of the following nuclei: ^{14}B, ^{15}C, ^{17}C and ^{19}C. Both nuclear and Coulomb dissociations were investigated using Be and Ta targets, except in the Coulomb dissociation of ^{17}C for which the background could not be removed. Little is known about the two heavy carbon isotopes and our data allow only a tentative interpretation.

The broad parallel momentum distribution obtained from the one-neutron nuclear breakup of ^{17}C shows no halo formation in this nucleus. With a separation energy of 0.73 MeV, this suggests a halo suppression due to the centrifugal barrier. Indeed, the spin-parity of the ^{17}C ground state is not well established, and shell model calculations indicate that the $1/2^+$, $3/2^+$, and $5/2^+$ levels are very close. A calculation using parentage coefficients obtained from the shell model gives the best agreement with the data for spin-parity of $3/2^+$ arising from *s*- and *d*-state neutrons coupled to the first

2^+ excited state of ^{16}C. However, this agreement is still uncertain due to the large error bars on the data. Clearly, better statistics would be desirable in order to distinguish the shape of the parallel momentum distribution and make a more sensible comparison to the calculations.

With our previous measurement on the nuclear breakup of ^{19}C on Be target [2], this experiment completed the preliminary program by observing its one-neutron Coulomb breakup on a Ta target. The observed width is very similar in both breakup processes. The analysis of these data is complicated by the large uncertainty on the mass of this nucleus, and further experimental progress in that direction would be welcome. As in the case of ^{17}C, the ground state properties of ^{19}C are not well known, and shell model predictions vary from one interaction to another. The nuclear breakup data do not seem to be consistent with an s ground state coupled to the ground state of ^{18}C. Rather, an $l=0$ ground state coupled to the first 2^+ excited state of ^{18}C seems to give the best agreement with the data, although a large leeway is allowed by the large error bars on both calculations and data.

For ^{11}Be, the best studied case of a single-neutron halo in an $l=0$ state, the Coulomb dissociation cross section has essentially full single-particle strength, and the comparisons in [7,18] suggest a spectroscopic factor of the order of 0.8, consistent with 10–20 % of the ^{10}Be $(2^+) \otimes 0d_{5/2}$ component in the $1/2^+$ ground state. An interesting contrast to this is provided by the heavier analogs ^{14}B and ^{15}C that have firmly established assignments. They are also s-states, but the neutron separation energies are higher by factors of 2 and 2.4, respectively, and the quenching of ^{14}B and ^{15}C dissociation probabilities is, as discussed above, clearly much larger and suggests a return towards normal nuclei for which the major part of the electric-dipole strength is shifted to the region of the giant dipole resonance. There are two reasons why it is difficult to make quantitative evaluations of the quenching on the basis of the present data. The first is that the technique used here is expected to introduce acceptance effects that make the absolute Coulomb cross section uncertain and the second is that the smaller Coulomb cross section makes it necessary to correct for the nuclear dissociation, which clearly must contribute also for the tantalum target. The conclusion is that the shapes of the momentum distributions confirm the picture that has emerged from studies of ^{11}Be and other halo states, but that more precise experiments with improved techniques are required are in order to understand the absolute cross sections.

ACKNOWLEDGMENTS

The authors are indebted to H. Esbensen for providing the Coulomb breakup calculations. This work was supported by NSF Grant No. PHY95-28844.

[1] J.D. Goss, A.A. Rollefson, C.P. Browne, R.A. Blue, and H.R. Weller; Phys. Rev. C **8**, 514 (1973).
[2] D. Bazin, B.A. Brown, J. Brown, M. Fauerbach, H. Hellström, S.E. Hirzebruch, J.H. Kelley, R.A. Kryger, D.J. Morrissey, R. Pfaff, C.F. Powell, B.M. Sherrill, and M. Thoennessen, Phys. Rev. Lett. **74**, 3569 (1995).
[3] E.K. Warburton and B.A. Brown, Phys. Rev. C **46**, 923 (1992).
[4] Z. Ren, Z.Y. Zhu, Y.H. Cai, and G. Xu, Nucl. Phys. **A605**, 75 (1996).
[5] R. Serber, Phys. Rev. **72**, 1008 (1947).
[6] B. Lohmann and E. Weingold, Phys. Lett. **86A**, 139 (1981).
[7] R. Anne, S.E. Arnell, R. Bimbot, H. Emling, D. Guillemaud-Mueller, P.G. Hansen, L. Johannsen, B. Jonson, M. Lewitowicz, S. Mattsson, A.C. Mueller, R. Neugart, G. Nyman, F. Pougheon, A. Richter, K. Riisager, M.G. Saint-Laurent, G. Schrieder, O. Sorlin, and K. Wilhelmsen, Phys. Lett. B **250**, 19 (1990).
[8] C.A. Bertulani and K.W. McVoy, Phys. Rev. C **46**, 2638 (1992).
[9] T. Kobayashi, O. Yamakawa, K. Omata, K. Sugimoto, T. Shimoda, N. Takahashi, and I. Tanihata, Phys. Rev. Lett. **60**, 2599 (1988).
[10] N.A. Orr, N. Anantaraman, S.A. Austin, C.A. Bertulani, K. Hanold, J.H. Kelley, R.A. Kryger, D.J. Morrissey, B.M. Sherrill, G.A. Souliotis, M. Steiner, M. Thoennessen, J.S. Winfield, J.A. Winger, and B.M. Young, Phys. Rev. C **51**, 3116 (1995).
[11] J.H. Kelley, S.M. Austin, A. Azhari, D. Bazin, J.A. Brown, H. Esbensen, M. Fauerbach, M. Hellström, S.E. Hirzebruch, R.A. Kryger, D.J. Morrissey, R. Pfaff, C.F. Powell, E. Ramakrishnan, B.M. Sherrill, M. Steiner, T. Suomijärvi, and M. Thoennessen, Phys. Rev. Lett. **77**, 5020 (1996).
[12] P.G. Hansen, Phys. Rev. Lett. **77**, 1016 (1996).
[13] H. Esbensen, Phys. Rev. C **53**, 2007 (1996).
[14] K. Hencken, G. Bertsch, and H. Esbensen, Phys. Rev. C **54**, 3043 (1996).
[15] B.M. Sherrill, D.J. Morrissey, J.A. Nolen, Jr., and J.A. Winger, Nucl. Instrum. Methods Phys. Res. B **56&57**, 1106 (1991).
[16] B.L. Cohen, Rev. Sci. Instrum. **30**, 415 (1959).
[17] J.H. Kelley, Sam M. Austin, D. Bazin, T. Kubo, and B.M. Sherrill, Nucl. Instrum. Methods Phys. Res. A **386**, 492 (1997).
[18] R. Anne, R. Bimbot, S. Dogny, H. Emling, D. Guillemaud-Mueller, P.G. Hansen, P. Hornshøj, F. Humbert, B. Jonson, M. Keim, M. Lewitowicz, P. Møller, A.C. Mueller, R. Neugart, T. Nilsson, G. Nyman, F. Pougheon, K. Riisager, M.G. Saint-Laurent, G. Schrieder, O. Sorlin, O. Tengblad, and K. Wilhelmsen Rolander, Nucl. Phys. **A575**, 125 (1994).
[19] L.K. Fifield, J.L. Durell, M.A.C. Hotchkis, J.R. Leigh, T.R. Ophel, and D.C. Weisser, Nucl. Phys. **A385**, 505 (1982).
[20] A. Ozawa, G. Raimann, R.N. Boyd, F.R. Chloupek, M. Fujimaki, K. Kimura, H. Kitagawa, T. Kobayashi, J.J. Kolata, S.

Kubono, I. Tanihata, Y. Watanabe, and K. Yoshida, Nucl. Phys. **A592**, 244 (1992).

[21] D. Ridikas, M.H. Smedberg, J.S. Vaagen, and M.V. Zhukov, Europhys. Lett. **37**, 385 (1997).

[22] F.M. Marqués, E. Liegard, N.A. Orr, J.C. Angélique, L. Axelsson, G. Bizard, W.N. Catford, N.M. Clarke, G. Costa, M. Freer, S. Grévy, D. Guillemaud-Mueller, G.J. Gyapong, F. Hanappe, P.G. Hansen, B. Heusch, B. Jonson, C. Le Brun, F. R. Lecolley, F. Lefebvres, M. Lewitowicz, G. Martínez, A.C. Mueller, T. Nilsson, A. Ninane, G. Nyman, B. Petersen, F. Pougheon, K. Riisager, M.G. Saint-Laurent, Y. Schutz, M. Smedberg, O. Sorlin, L. Stuttgé, and D.D. Warner, Phys. Lett. B **381**, 407 (1996).

[23] G. Audi and A.H. Wapstra, Nucl. Phys. **A565**, 1 (1993).

[24] C.A. Bertulani and G. Baur, Nucl. Phys. **A480**, 615 (1988).